Further Development of a High Pulse-Energy LED at 4 kHz for Volumetric Particle Tracking Velocimetry and a Demonstration Using 32 Such LED Units

H. Abitan[1,*], Y. Zhang[1], B. Edelsten[1], N. S. Jensen [1], C. M. Velte[1]

1: Dept. of Civil and Mechanical Engineering, The Technical University of Denmark, Denmark
*Corresponding author: haiab@dtu.dk

Keywords: Volumetric PTV, 3D-PTV, LED.

ABSTRACT

In 2022, we reported at the 20th Lisbon symposium on the development of $460\,nm$ LED specifically designed for illumination in volumetric Particle Tracking Velocimetry (PTV). At that time, our pulsed LED unit emitted light with a 6° divergence beam and a top-hat power cross section, producing $20\,\mu s$ pulses at a $4\,kHz$ repetition rate and a $0.15\,mJ$ pulse energy. Since then, we have been improving the efficiency of this LED. Currently, our LED unit emits a beam with similar specifications but with a pulse energy up to $0.65\,mJ$, which is 4.3 times more than the previous LED unit. We improved the efficiency of the electrical driver by further decreasing the footprint of the SMD circuitry and by using higher quality electronic components. Additionally, we replaced the aluminium pin fin heat sink with a copper pin fin heat sink and we characterized the thermal dissipation. Using SolidWorks, we integrated the electric driver, the copper heat sink and the collimating optics into a compact mechanical casing. These improvements resulted in an LED unit with greater overall efficiency, a larger pulse energy and a volume footprint that is half the the size of the previous design. Furthermore, we constructed four batteries of these LEDs, with each battery containing eight LED units. Here, we report on our improvements to the LED unit and our considerations in its development. Additionally, we describe preliminary results of a 3D-PTV experiment with Helium Filled Soap Bubbles (HFSB), which were illuminated by the four LED batteries.

1. Introduction

In the past two decades, LEDs manufacturers have been developing LEDs with improved spectral intensity $[W][sr]^{-1}[Hz]^{-1}$ while decreasing sharply their cost per Watt output (at the present, it is about 7 EURO per Watt). Researchers in the field of flow visualization and velocimetery caught-up and identified the benefits of LEDs as illumination sources for their experiments. Beside their lower price, LEDs has two additional advantages over lasers: LEDs illumination show no speckles in the images (due to the low coherence of the LED light) and their light pulses comply accurately with the pulses of the driving current. This current compliance means that by using a standard

electric generator, one can generate short light-pulses, down to several nanoseconds of pulse duration. This can be done within a large frequency band (sub Hz to MHz) and with low pulse jitter. Such a pulsed light source is ideal for flow visualization and velocimetry.

Table 1 is a summary of selected applications of LEDs in flow visualisation and velocimetry measurements in the past two decades. It shows the typical values of: Volume/Area Of Interest, (VOI/AOI), average pulse current $\langle i_p \rangle$, pulse duration τ, averaged pulse energy $\langle E_p \rangle$, and the repetition rate,f_{rep}. The last row indicates to the great potential of using LED illumination in large 3D-PTV experiments with Hellium Filled Soap Bubbles (HFSB) together with Shake The Box (STB) algorithm.

Table 1. Visualisation and Velocimetery Techniques with LEDs as the Illumination Source

Technique	AOI/VOI	$\langle i_p \rangle$ $[A]$	$\tau\,[\mu s]$	$\langle E_p \rangle$ $[mJ]$	f_{rep} [Hz]
Shadowgraphy					
(Broder & Sommerfeld, 2007)	$78\,cm^2$	-	$50-70$	-	$0.3-1\,kHz$
Schlieren					
(Buttsworth & Ahfock, 2003)	$78\,cm^2$	5	$1.5-38$	$\approx 10^{-1}$	-
MicroPIV					
(Nasibov et al., 2013)	$0.01\,mm^2$	$0.7-35$	10	≈ 0.05	23
PIV					
(Willert et al., 2010)	$0.7\,cm^2$	$2-50$	$2-20$	0.4	$1-2\,kHz$
PTV					
(Huhn et al., 2018)	$6\cdot 10^5\,cm^3$	-	3000	≈ 72	29

Three years ago we took on the development of an LED source for volumetric PTV using $15\mu m$ Mie scattering Air Field Soap Bubbles (AFSB). In 2022 we reported at the 20th Lisbon symposium (Abitan et al., 2021) on a prototype LED unit that generated a $20\,\mu s$ pulse with $0.15\,mJ$ of pulse energy at a $4\,kHz$ repetition rate. We used this LED to detect $15\mu m$ Mie scattering AFSB (at the present we have doubts regarding the nature and the actual diameter of the AFSB).

At the present, our $460\,nm$ LED unit is compact: it has a small volume footprint of $100\times 100\times 80\,mm^3$. It is powered by a standard wall plug DC power supply ($5.5\,V, 5\,A$). It is cooled by passive air and it is directly mounted into a ball joint for easy pointing of the beam. The LED unit emits light with a 6° beam divergence angle and a top-hat power cross section. It generates $20\,\mu s$ pulse-width at a $4\,kHz$ rate and a pulse energy up to $0.65\,mJ$. We constructed 32 units of such LEDS and we used them to illuminate a $16128\,cm^3$ VOI in a 3D-PTV experiment with Helium Filled Soap Bubbles (HFSB) as trace particles.

2. Electric and Electro-Optics of the LED

2.1. LED power Vs. Current

The output power, P_{LED}, from a typical LED unit can be modeled as (Coldren et al., 2012; Schubert, 2006; Abitan et al., 2022):

$$P_{LED} = \eta_i \eta_r \eta_c \eta_{gc} \frac{h\nu i}{q} = \eta_{oa} \frac{h\nu i}{q} \tag{1}$$

where the efficiency factors $\eta_i, \eta_r, \eta_c, \eta_{gc}$ and η_{oa} are shortly explained and their values are given in Table 2.

Table 2. The efficiency coefficient in LED

Symbole	Meaning	Value
η_i	injection current	0.95
η_r	radiadive	0.88
η_c	coupling	0.7
η_{gc}	gathering coupling	0.7
η_{oa}	overall efficiency$= \eta_i\eta_r\eta_c\eta_{gc}$.	0.41

Plugging into Equation 1 the values of the efficiency factors, the Plank constant $h = 6.6{\times}10^{-34}[J][Hz]^{-1}$, the electron charge $q = 1.6 \times 10^{-19}$ Coulomb, and the LED frequency $\nu = \frac{c}{\lambda}$ (where the LED wavelength $\lambda = 460\,nm$ and $c = 3 \times 10^8\,m/s$ is the speed of light in vacuum), we obtain:

$$P_{LED} = 2.6 \times 0.95 \times 0.7 \times 0.3 \times 0.7 \; = 0.41i = \eta_{oa} i \tag{2}$$

This equation for the optical power of our collimated optical output is linear with the current. We can use it to estimate that in order to obtain $20\,\mu s$ pulse with $1\,mj$ pulse energy, we would need to drive the LED with a current of $121\,A$. However this estimation does not consider efficiency drooping (Piprek, 2011) in GaN LEDs, which is implied through the radiation coefficient η_r. The Luminus PT-121-B has an area of $12\,mm^2$. If we drive it at $121\,A$, it corresponds to current density of $1008\,A/cm^2$ where efficiency drooping is present (Piprek, 2020).

2.2. The Electric Circuitry for Over Driving

One can understand the operation of our LED driver by examining Figure 1:

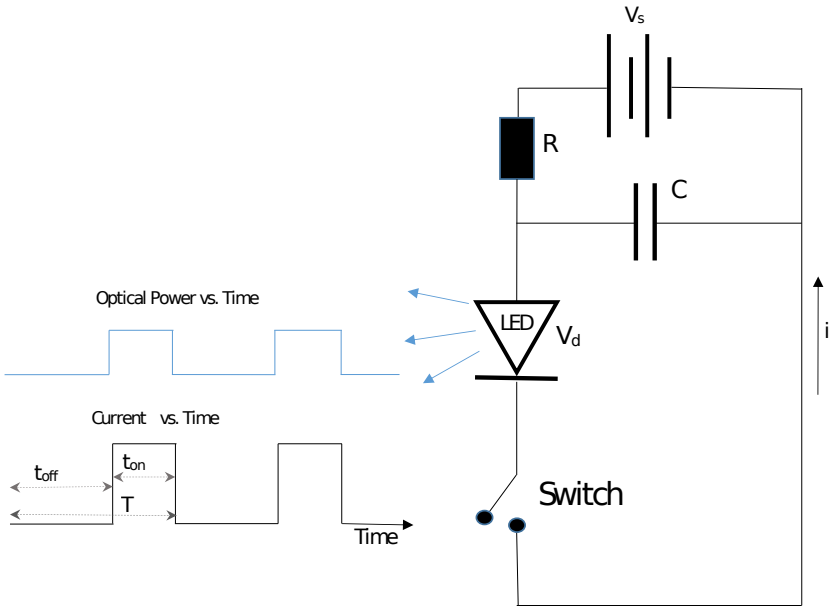

Figure 1. The basic structure of the LED driving circuit

The switch is turned on for t_{on} of a second and then it is turned off for t_{off} of a second over a period $T = t_{on} + t_{off}$. This happens repeatably with frequency $f_{rep} = \frac{1}{T}$. When the switch is open for t_{off} of a second, current flows from the power supply V_s to charge the capacitor C. After the time t_{off}, the switch is closed for t_{on} of a second. In this time interval, current flows through the LED. The current comes simultaneously from the power supply and from the capacitor. The switch is a MOSFET transistor. It acts as a fast electric switch. The transition time from t_{off} to t_{on} can be down to several tenth of nanoseconds. We use a gate driver in order to control the switching with high accuracy.

The electric circuit to over drive our LED in a pulse mode was inspired from the design reported by Willert et al. (2010). However, our circuits were done with Surface Mounted Device (SMD) technology, in order to reduce inductance noise and circuit footprint. Additionally, we added a circuit to protect the LED from over heating and another circuit to control the slew rate of the current pulse during the transition time. Thus protecting the LED from thermal damage and over shooting currents.

2.3. Optic and Electro-Optics of the LED

We characterized the optical output from our LED with three types of measurements:

- First, we measure the average optical power emanating from the LED, $\langle P_{LED} \rangle$, with an optical power meter (Centauri, High End Power Meter with 50 W Thermopile sensor, mks Ophir). The average pulse energy equals to the average optical power divided by the pulse repetition

rate, f_{rep}:

$$\langle E_p \rangle = \frac{\langle P_{LED} \rangle}{f_{rep}} \tag{3}$$

- Second, we measured the temporal pulse shape of the light pulse of the LED, $P_{LED}(t)$, using a silicon Surface Mount Device (SMD) Photo Diode (PD), SPD19-C. It has $6\,ns$ responsivity and half sensitivity over an angle of $80°$. The photocurrent signal from the PD was converted to a voltage signal by a transmitter of photocurrent into a voltage signal into the range of $0-5\,V$ (Voltcon $0-5$). A digital scope (HAMEG HMO 15 22) showed this temporal voltage signal.

- Third, we used a digital control DC power supply (RS-pro, RS-300 5D) to drive the LED. This power supply has an adjustable voltage and a controlled compliance current. Hence, we could control the average driving current $\langle i \rangle$ that the LED draws. This is a useful feature. Our LED consumes most of the current (the other circuits for the MOSFET gate driver and the thermal protection have negligible current consumption of few milliampere). Accordingly, assuming the current into the diode is a train of square pulses with pulse duration τ, as shown in Figure 1, the averaged peak current $\langle i_p \rangle$ is given by:

$$\langle i_p \rangle = \frac{\langle i \rangle}{\tau f_{rep}} \tag{4}$$

The measurements of the optical features of our LED are summarized Figures 2-4: Figure 2 shows the averaged pulse energy, $\langle i_p \rangle$, vs. the driving currents of the power supply:

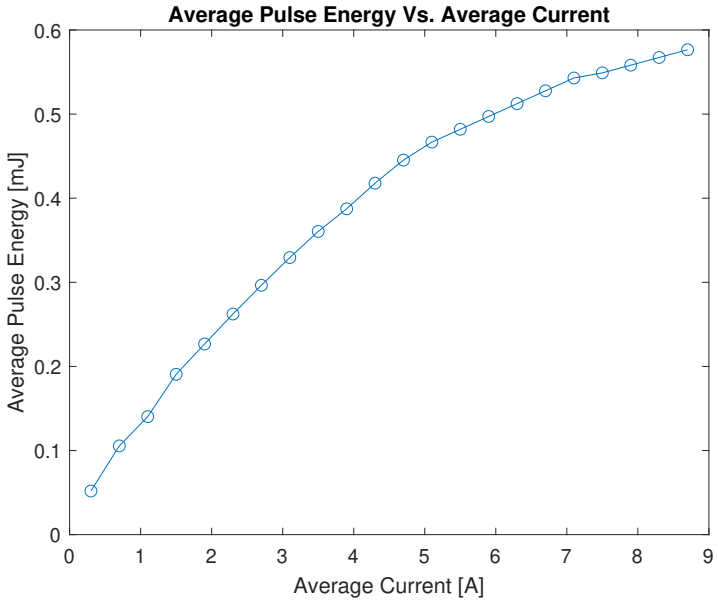

Figure 2. Average pulse energy vs. average driving current measured by a thermopile power meter

One can see in Figure 2 that the averaged pulse energy is linear with the average driving current up to about $4A$. At larger driving currents, we can see a drop in the slope, which represent the power efficiency. This is due to the overheating of the LED and due to gain drooping.

Figure 3 shows a scope measurement for pulse power vs. time, taken by our PD at $1.5\,A$ average current (and $V_s = 5.5\,V$). It corresponds to an average peak current $\langle i_p \rangle = \dfrac{1.5}{20 \cdot 10^{-6} \times 4 \cdot 10^{3}} = 18.75\,A$

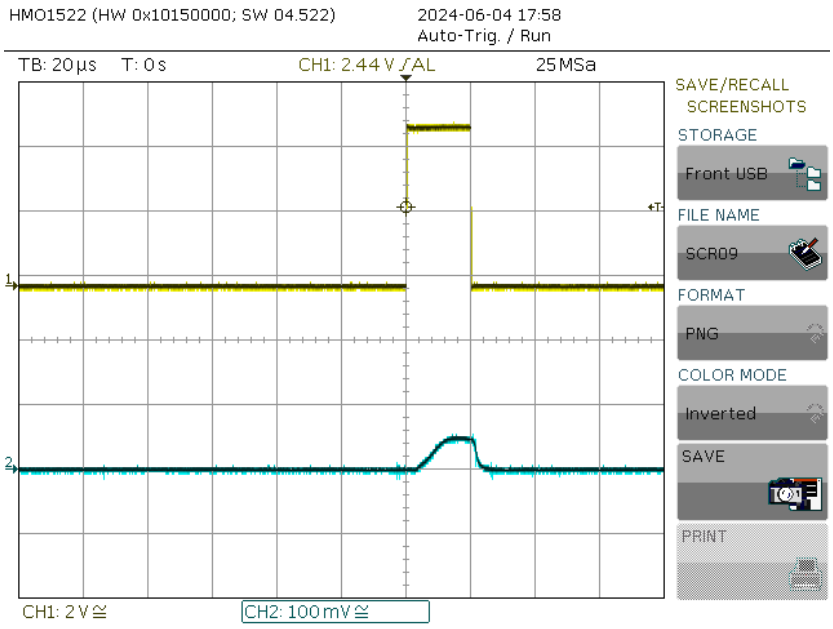

Figure 3. The top scope trace (yellow) is the pulse of the pulse generator, which controls the the MOSFET switch. The lower scope trace (blue) shows the light pulse of the LED as measured by our photodiode

Note that the temporal pulse current i_p, is constant, after reaching its peak. When we drive the LED with $1.6\ A$, we start to see that i_p decreases during the pulse interval. This is clearly shown in Figure 4 where the LED is driven by $5.1\ A$ average current which corresponds to $\langle i_p \rangle = 63.75\ A$:

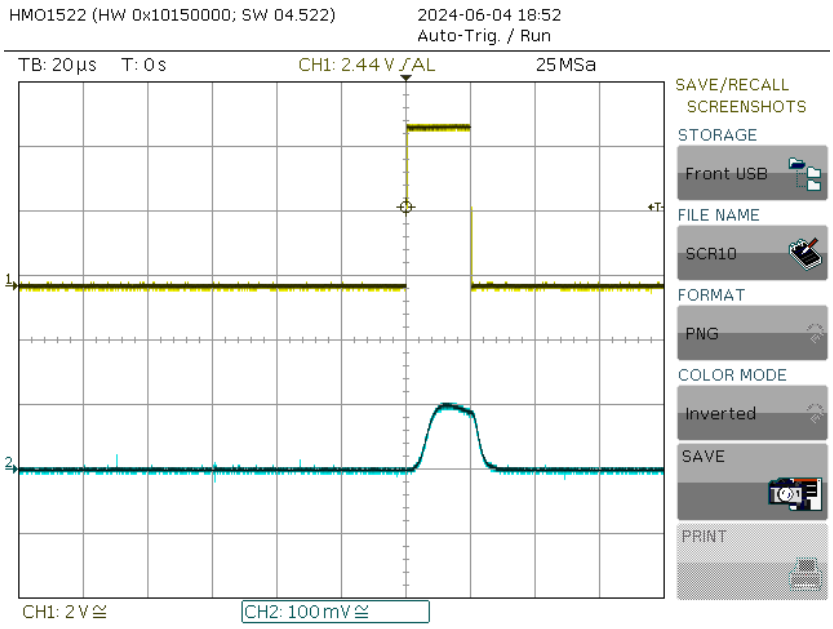

Figure 4. Top scope trace (yellow) is the trigger pulse for the MOSFET. The lower scope trace (blue) shows the light pulse of the LED at 5.1 average driving current as measured by a photodiode. Note that the peak current i_p drops after reaching its maximum. This is due to gain drooping and thermal effects

These measurements (with passive air cooling), convinced us that if we will drive the LED with less than $4\,A$, we could use passive air cooling, use a standard wall plug DC power supply, and then avoid the complication of thermal load and high density currents and the fall in the overall efficiency of the LED (Piprek, 2020).

3. Heat Management in a High Power Pulsed LED

The manufacturer (Luminus) of our LED chip (PT-121-B-L11) guarantees 60,000 hours of LED operation when the junction temperature is kept bellow $120\,°C$. It was therefore important for us to assure that the heat load upon the LED will not damage its junction.
The source of the heat load is the driving electric current. When the LED runs with a continuous current, the LED consumes electric power $P = iV_d$. Part of this power is converted into optical power, P_{LED}, as is shown in Equation 1. This power escapes the LED as a useful output light. It does not contribute to the heat load of the LED. Therefore the power load is $P_{Diss} = V_d i - \eta_{oa} i$. Since our LED runs in a pulsed mode, the average power load $\langle P_{Diss} \rangle$ can be expressed as:

$$\langle P_{Diss} \rangle = (V_d - \eta_{oa})\, \tau f_{rep} \langle i_p \rangle = (V_d - \eta_{oa}) \langle i \rangle \tag{5}$$

3.1. Measurements of Temperatures on the LED

The Luminus LED chip has a built in thermistor (Murata NCP18XH103J03RB) at the proximity of the LED junction as illustrated in Figure 6. Luminus supplies data for the maximal allowed temperature on that thermistor for a given power load: When the power load in the LED junction is $12.5\,W$ ($3.5\,A$ and $V_d = 4\,V$), the temperature at the junction will be $10\,^{\circ}C$ higher.
The temperature on the LED thermistor was measured as followed:

- We connected the LED thermistor R_{ther} in series with a reference resistor $R_{ref} = 4.7k\Omega$ and connected them with a constant 5 volt DC power supply. Kirchhoff analysis of this circuit gives that the resistance of the thermistor depends on the voltage across the thermistor as:$R_{ther} = \dfrac{V_{R_t} 4700}{5 - V_{R_{ther}}}$
- We used a National Instrument NI-9215 to measure the voltage across the thermistor at a 4 kHz sampling rate.
- We used 16 data sets of resistance and temperature pairs (supplied by Luminus) to build an approximated function of the temperature vs. the resistance. We used this function to convert the voltage data from the I-9215 into temperature data.

3.2. The Thermal Load upon the LED Unit in 3D-PTV Experiments

Our 3D-PTV experiments requires an intermittent operation of the LED: The LED is pulsing for Δt_{on} seconds, then the LED is turned off for Δt_{off} seconds (the time interval which the camera transfers the images into a digital storage) and then a repeating measurement cycle begins.
During Δt_{on}, the current through the LED juncion generates the heat load: $\langle P_{Diss} \rangle \, \Delta t_{on} \, J$. This heat load flows from the LED junction into the copper base of the LED and from there into the heat sink and into the ambient air. Not surprisingly, during the time Δt_{off}, heat continues to dissipate into the ambient air from the heat sink (this is passive air cooling). If we wait long enough, the passive air cooling could remove completely the generated heat load from the LED during Δt_{off} .

Figure 5 contains three plots. Each plot shows the temperature of the LED thermistor (see Figure 6). The measurements start just before the LED is turned on. Then the LED is pulsing for Δt_{on} seconds: That is, for $2, 4$ and 10 seconds in each plot respectively. The temperature is monitored also during Δt_{off}, until the thermistor regains the initial temperature.

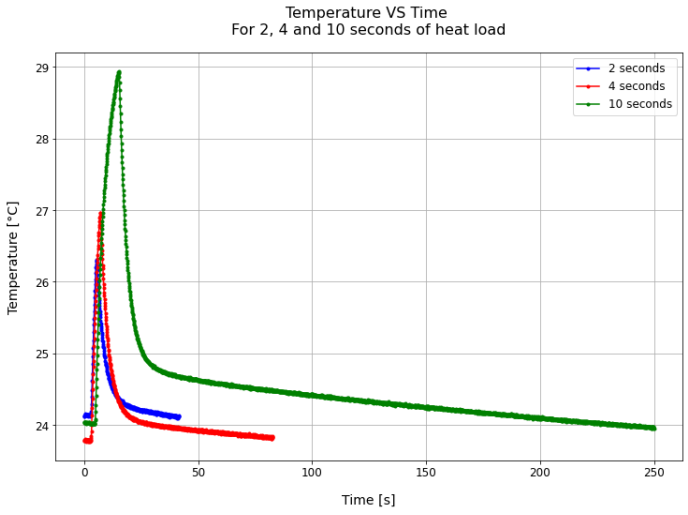

Figure 5. The temperature at the LED's thermistor vs. time in three experiments: The LED is pulsed for 2,4 and 10 seconds and the temperature is measured until the LED regains the initial temperature. The LED runs at $4\,kHz$ repetition rate, $20\mu s$ pulse width and power load of $12.58\,W$

We see in Figure 5 that for $\Delta t_{on} = 2$ seconds, the initial temperature is regained after 40 seconds. For $\Delta t_{on} = 4$ seconds, the initial temperature is regained after 80 seconds and for $\Delta t_{on} = 10$ seconds, the initial temperature is regained after 250 seconds. These measurements were taken at room temperature of $21\,^{\circ}C$. The LED was pulsed at $4\,kHz$ with $20\,\mu s$ pulse duration with average power load $\langle P_{Diss} \rangle = 12.58\,W$. These time intervals gives us a guiding for how we can operate the LED safely while using passive air cooling.

Figure 6 is a cross section of the LED mounted on top of a copper fin pin heat sink.

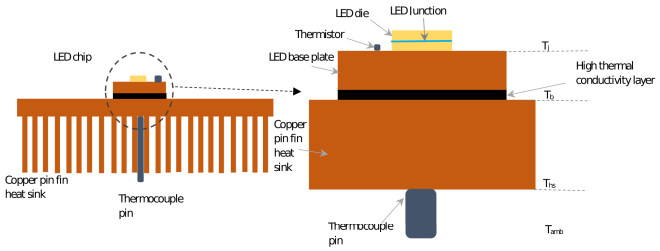

Figure 6. A cross section of the LED chip mounted on a base plate. The base plate is attached to a pin fin heat sink with a high thermal conductivity layer between them

It is of practical interest to estimate the temperature at the LED junction (without computer simulations) when the LED is pulsing for a long period, i.e., $\Delta t_{on} \gg 1$.

As the heat flows from a high temperature surface towards a low temperature surface, the amount of heat ΔQ that will flow per unit time Δt will be proportional to the cross section area A, the temperature difference and reciprocally to the distance between the two planes Δx.

$$\frac{\Delta Q}{\Delta t} = \kappa \frac{A}{\Delta x} \Delta T \tag{6}$$

where the proportionality constant, κ, is called the heat conductivity. In the field of thermal engineering , it is customary to rearrange Equation 6 and write it as

$$\Delta T = R_\theta \frac{\Delta Q}{\Delta t} = R_\theta \langle P_{Diss} \rangle \tag{7}$$

where R_θ is called the thermal resistance.

Figure 6 depicts the cross section of the LED unit. We can see the top layer of the LED junction, just bellow it, the layer of the copper base. At their boundary there is temperature T_j. Then there is a layer of a high thermal conductivity between the base plate and the heat sink (it has effectively the same temperature T_j). At the bottom of the heat sink there is the temperature T_{hs}. Each layer has its characteristic heat conductivity and its corresponding thermal resistance. The temperature difference between the two external layers (the LED junction and the ambient air) can be estimated by considering the total series thermal resistance (as in Ohm's law).

Table 3 summaries the notation for temperatures at four points of interests and the thermal resistance for each layer between these points.

Table 3. Notation for the temperatures at four points of interest, the corresponding thermal resistances and their values.

Symbol	Meaning	Value
T_j	temperature at the LED junction when $\langle P_{Diss} \rangle = 12.58\,W$	$T_{ther} + 10\,^\circ C$
T_{hs}	temperature at the heat sink	
T_{ther}	temperature at the thermistor	
T_{amb}	temperature of ambient air	$22\,^\circ C$
$R_{\theta:j-b}$	thermal resistance between the junction and the base plate	$0.4\,^\circ C/W$
$R_{\theta:b-hs}$	thermal resistance between the base plate and the heat sink	$0.1\,^\circ C/W$
$R_{\theta:hs-amb}$	thermal resistance between the heat sink and the ambient air	$3\,^\circ C/W$

The temperature difference between the LED junction and the ambient temperature is due to the sum of all of the thermal resistances times the heat load:

$$T_j - T_{amb} = (R_{\theta:j-b} + R_{\theta:b-hs} + R_{\theta:hs-amb}) \langle P_{Diss} \rangle \tag{8}$$

Plugging the values of the thermal resistances as given in table 3 and taking the ambient temperature to be $22^\circ C$:

$$T_j = 22 + R_\theta \langle P_{Diss} \rangle = 22 + 3 \langle P_{Diss} \rangle \tag{9}$$

When we run the LED continuously in the pulsed mode with $\langle i \rangle = 3.5\,A$, the optical power is $1.42\,W$. Since the LED voltage is $V_d = 4\,V$, the dissipated power is $\langle P_{Diss} \rangle = 3.5 \cdot 4 - 1.42 = 12.58\,W$. The temperature at the junction is: $22 + 2.5 \cdot 12.58 = 59.74\,^{\circ}C$.

Figure 7 shows the measured temperature at the LED thermistor vs. time when $\Delta t_{on} = 1500$ seconds and $\Delta t_{off} = 6500$ seconds. After 1500 seconds (25 minutes) of continuous pulsing, the temperature at the LED Junction is about $82 + 10 = 92\,^{\circ}C$. The measured temperature is larger than our estimation by 50%. It could be that the value of the thermal resistance we use for our passive heat sink is not accurate (we took them from data sheets of the Luminous).

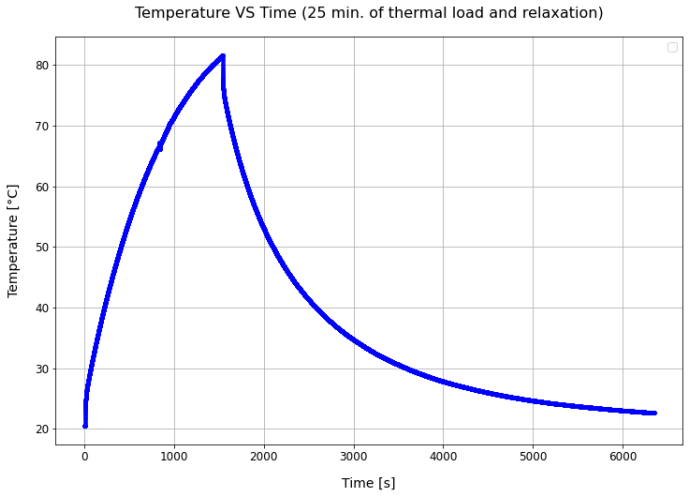

Figure 7. The temperature at the LED's thermistor vs. time in three experiments: The LED is pulsed for 2,4 and 10 seconds and the temperature is measured until the LED regains the initial temperature. The LED runs at $4\,kHz$ repetition rate, $20\mu s$ pulse width and $3.5\,A$ average drive current

We can see that the temperature at the thermistor keep rising but with a decreasing rate. The temperature will stabilize when the rate of the heat load will equal to the rate of the heat dissipation by the heat sink into the ambient air. However we stoped the measurements after $1500\,s$. The temperature at the LED thermistor returned to its initial temperature after $6500\,s$.
These measurement helped us to establish that our heat dissipation is satisfactory. In order to assure that our LED junction will not be overheated above $120\,^{\circ}C$, we added a protection circuitry that shuts the LED when its thermistor temperature reaches $80\,^{\circ}C$.

4. Application of the LEDs in Volumetric PTV

We conducted a 3D-PTV experiment with HFSB as trace particles in order to measure the large scale turbulent flow from a jet with a $1\,cm$ nozzle diameter (Zhang, 2024). The exit velocity of the jet flow can be set between $1.46 - 14.6\,m/s$, corresponding to Reynolds numbers ranging between $\sim 10.000 - 100.000$. Figure 8 depicts the experimental setup.

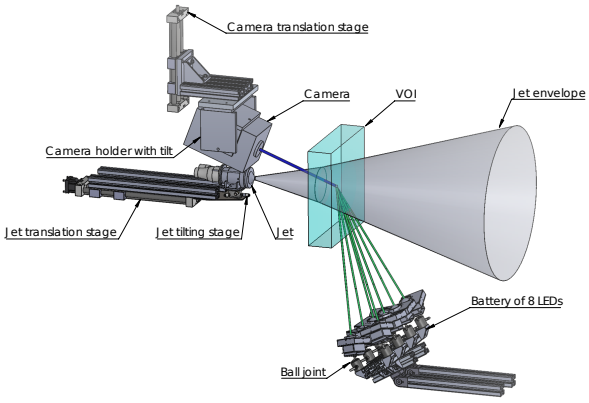

Figure 8. A scaled drawing of the main elements in our 3D-PTV experiment

The full setup consists of 4 cameras, 1 jet and 4 batteries of LEDs. For illustrative purposes, figure 8 shows only one camera and one battery of LEDs. All supporting structures have been excluded.

The jet is mounted on a tilting stage, allowing for the jet center axis to be rotated in both the vertical and horizontal plane, thereby making it possible to align the jet stream to the rest of the setup. To observe the flow further upstream or downstream, the jet tilting stage is mounted on a motorized translation stage that allows for the jet to be moved $300\,mm$ along the jet center axis. Each cameras is mounted to tilting the holders, allowing for the cameras to be pointed to the center of a VOI at different distances along the jet axis. The cameras are mounted upon motorized translation stages that can move the cameras radially closer and further away from the jet center axis, thereby, allowing for automatic selection of the volume of interest. The 4 LED batteries are each made up of 8 LEDs. Each LED is mounted on a ball joint, so that each individual LED can be pointed towards the center of the VOI, independently of the other LEDs. The LEDs have passive air cooling, in order to avoid inflow of air into the VOI. All 4 LED batteries are mounted on a structure that can be translated along the jet center axis.

4.1. Estimation of the Required Pulse Energy

When we conduct volumetric 3D-PTV experiments with Mie trace particles in a VOI that has a large cross section area, the power of the image of the particle will be low (the Mie scattering factor is of the order of $\approx \cdot 10^{-16}\,cm^2$). To improve the signal, we can increase the pulse energy of the light source or work with a smaller VOI and focus the same amount of light into a smaller cross section area. Another way to increase the signal is to arrange the experimental configuration so that the Mie scattering is scattered in forward scattering towards the CMOS camera. Since

the light beam of our LEDs is directional with 6° divergence angle and a top-hat power cross section, we can illuminate the Mie scattering of the VOI in forward scattering. For example the Mie scattering at 60° forward scattering is 18 times larger than the Mie scattering signal with right angle illumination. We used Solidworks to explore the positioning of the LEDs batteries, jet and cameras in order to benefit from large forward Mie scattering, as is illustrated in Figure 9.

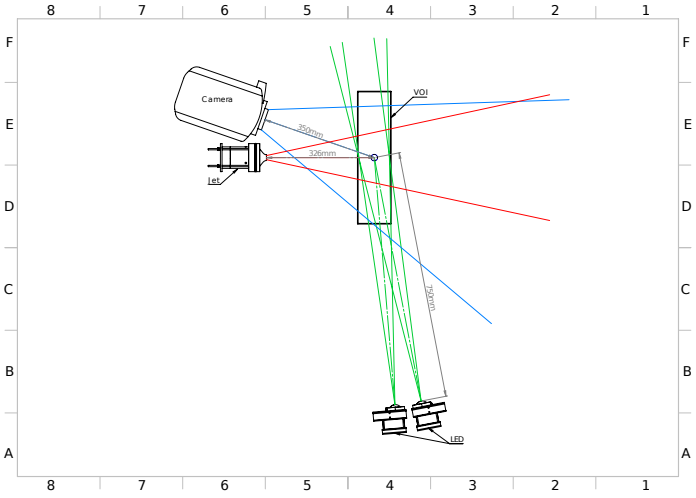

Figure 9. A cross section of the 3D-PTV experiment. The blue cone, with its apex within the camera, illustrates the angle of view of the camera (42°). The jet has also a conical envelope (red cone) with a typical apex angle. The LED has a beam with a 6° divergence angle (green cone) and a top-hat power cross-section. It is useful feature in for forward Mie scattering. The LED and its beam are placed outside the viewing cone of the camera

We estimated the signal current, i_S, in a CMOS camera by using an expression (Abitan et al., 2024) that is adapted for a light beam with a top-hat cross section:

$$i_S = \frac{E_p}{A\tau} \times (1-L) \times e^{-\alpha z_l} \times \sigma(\theta) \times \frac{D_a^2}{16 z_o^{+2}} \times e^{-\alpha z_o^{+}} \times T(\lambda) \times FFR(CoC) \times R(\lambda) \quad (10)$$

The symbols in Equation 10, their meaning and values are shown in Table 4:

Table 4. Coefficient, their meaning and their values for calculating the signal level with equation 10

Coefficient	Meaning	Value
E_p	pulse energy $[mJ]$	1.8
A	cross section area of the LED beam $[cm^2]$	$10 \times 15 = 150$
τ	pulse duration $[\mu s]$	20
L	beam guiding losses	negligible
α	optical loss coefficient for the seeded air $[cm^{-}1]$	negligible
$\sigma\,(60°)$	Mie scattering at $60°$ for $15\,\mu m$ particle diameter	$2 \cdot 10^{-15}$
R_s	Fresnel reflection at $60°$, sagittal plane	0.1
D_a	aperture diameter of the camera $[mm]$	3.18
z_o^+	distance from the camera lens to the far edge of the DoF $[mm]$	400
$T\,(\lambda)$	Fresnel's transmission of the camera lens at λ	0.8
$FFR(CoC)$	a factor due to the Circle of Confusion	0.04
$R\,(\lambda)$	Responsivity at λ of the CMOS camera	0.2

In order to estimate the signal from $15\,\mu m$ diameter Mie particle, we plug into Equation 10 the values that are given in table 4 and obtain a very small signal on the CMOS detector: about 0.0026 electron counts for one LED unit. It is clear from this estimation that our LED can not detect the signal (image) from a $15\,\mu m$ diameter Mie particle. We need to work with larger particles, such as HFSB.

In order to estimate the signal level for a HFSB, we remove the forth and the fifth factors from Equation 10 and replace it by the Fresnel's reflection factor R_s for $60°$ angle of incidence (the large HFSB are reflecting light according to geometric optics). It is clear that the signal (image of a particle) of a HFSB will be easily detected by the CMOS camera.

4.2. Results of Measurements

The experimental set-up of the LEDs and cameras are shown in Figure 10. To enhance light signal acquisition, forward scattering is implemented by adjusting the LEDs to face the cameras as much as possible. The seeding setup is located at the jet position.

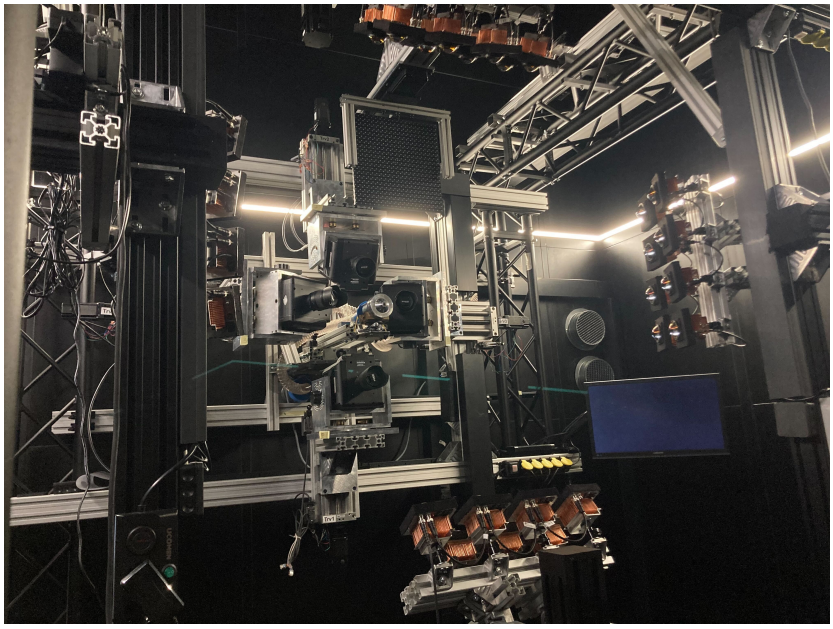

Figure 10. The experiment setup with jet, cameras and LEDs.

The LEDs are adjusted to illuminate the desired volume, facilitated by the movement of the calibration target. Subsequently, the bubbles are distinctly visualized within the illuminated volume, as depicted in Figure 11.

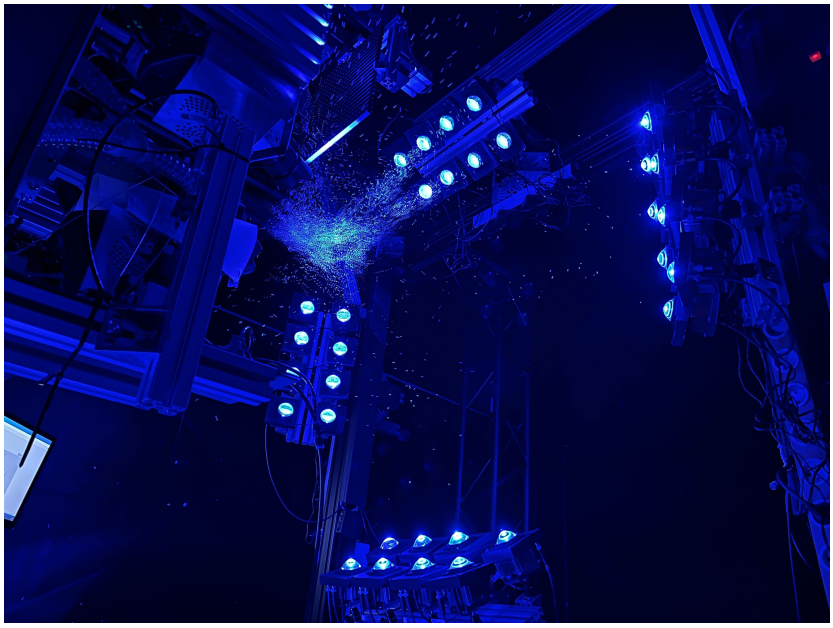

Figure 11. The 32 LEDs illuminate the VOI and the bubbles are clearly visible.

The VOI is $6250cm^3$ ($25cm \times 25cm \times 10cm$). However, due to the larger calibrated volume and larger illumination volume, the interpretation of the flow is larger than the VOI, and the effective

volume is $16128cm^3$ ($32cm \times 28cm \times 18cm$).

The image of one recording is shown in Figure 12. The signal intensity from the particles range from 130 counts to 600 counts, high enough to obtain particle tracks.

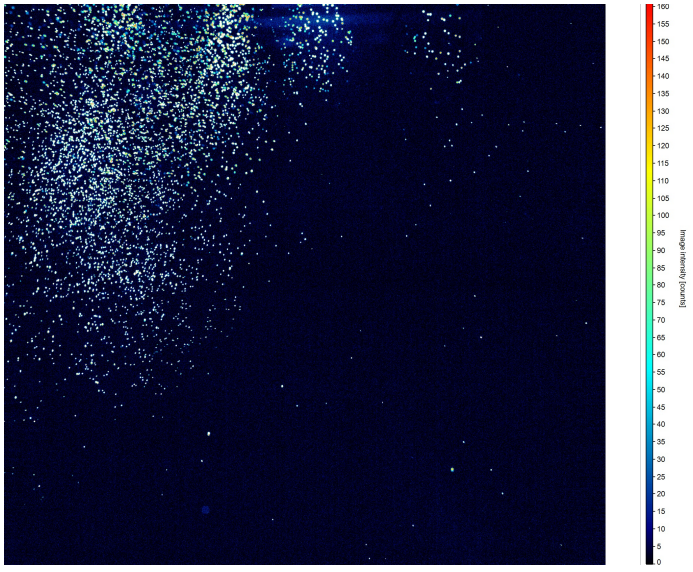

Figure 12. .

The recording was processed by Davis 10, and the Shake-The-Box algorithm was utilized to produce the particles tracks. One snapshot of the results is shown in Figure 13.

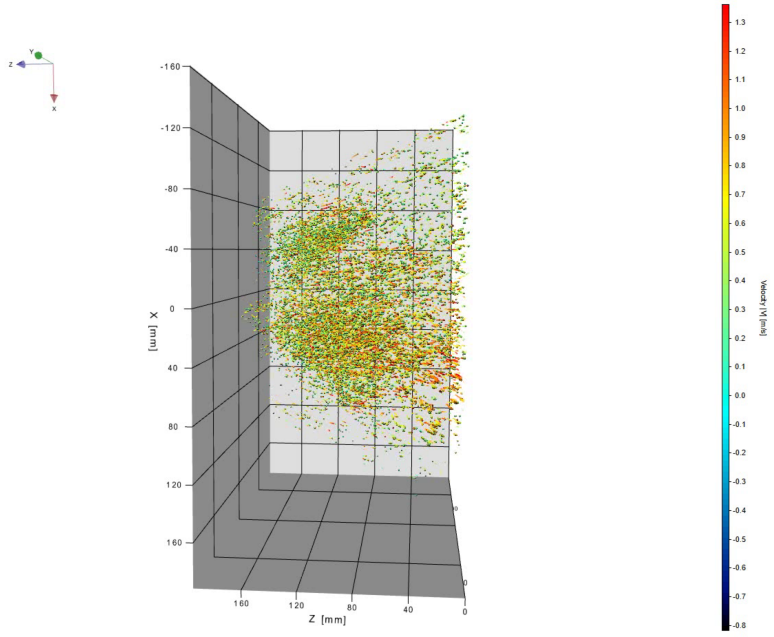

Figure 13. .

5. Conclusions

We developed a pulsed LED for 3D-PTV measurements. At the present, our $460\,nm$ LED unit is compact: it has a small volume footprint of $100 \times 100 \times 80\,mm^3$. It is powered by a standard wall plug DC power supply (since we built 32 units, the low cost of wall plug DC power supply at 5.5 V and 5 A was a consideration). It is cooled by passive air and it is directly mounted into a ball joint for easy steering of the beam towards the VOI. The LED unit emits a a light beam with 6° divergence angle and a top-hat power cross section. It generates $20\,\mu s$ pulse-width at a $4\,kHz$ pulse rate and pulse energy up to $0.65\,mJ$. We constructed 32 units of such LEDs and used them to illuminate a $6250cm^3$ VOI in a 3D-PTV experiment with Helium Filled Soap Bubbles (HFSB). We characterized the LED (average pulse energy over driving current, light pulse shape vs. time, and thermal load effect) and accordingly chose to operate the LED with a current that does not cause for meaningful thermal stress or gain degradation. This ensures durability of the LED for 60,000 working hours.

In the future we would like to:

- Explore active air and water cooling in order to increase the the average pulse energy $\langle E_p \rangle$.
- Investigate telescopic optics to focus the LED beam at points of interest.
- Improve the electrical circuit: add a mode of low power for safe alignment, indication LED for operation, interface with IoT and use optocouplers for triggering interface.

It seems likely that in the future, LED illumination will find use in large volume 3D-PTV experiments with HFSB.

Acknowledgements

H. Abitan and C. M. Velte acknowledges financial support from the Poul Due Jensen Foundation, grant No 2018-039: Financial support from the Poul Due Jensen Foundation (Grundfos Foundation) for this research is gratefully acknowledged. Y. Zhang and C. M. Velte acknowledge financial support from the European Research Council: This project has received funding from the European Research Council (ERC) under the European Unions Horizon 2020 research and innovation program (grant agreement No 803419).

Nomenclature

η	Efficiency Factor

i	Temporal Current[A]
c	speed of light in vacuum[M]/[s]
i_p	Peak Current of a Pulse [A]
$\langle i \rangle$	Average Current [A]
P_{LED}	LED Power [W]
$\langle P_{LED} \rangle$	Average LED Power [W]
$\langle P_{Diss} \rangle$	Dissipated Power [W]
$\langle E_p \rangle$	Average Pulse Energy [J]
f_{rep}	Pulse Repetition Rate [Hz]
T	wave period $[s]^{-1}$
Δt_{on}	Time Interval of measurement (LED is ON) [s]
Δt_{off}	Time Interval when LED is off while images are stored [s]
τ	Pulse Width [s]
V_d	Voltage on LED [V]
V_s	Voltage of Power Supply [V]
ΔQ	Heat [J]
Δt	Time Unit [s]
ΔT	Temperature Difference $[^\circ C]$
Δx	Distance [m]
A	area $[cm]^2$
R_θ	Heat Resistance $[^\circ C]$/[W]
κ	Heat Conductivity [W]/$[^\circ C]$[m]
R_{ther}	Thermistor Resistance [Ohm]

References

Abitan, H., Edelsten, B., Zhang, Y., Ribergård, L., & Velte, C. M. (2022). Optical and electrical considerations for developing pulsed high-power led for volumetric particle tracking velocimetry. In *Proceedings of the 20th international symposium on application of laser and imaging techniques to fluid mechanics.*

Abitan, H., Zhang, Y., Ribergår, S. L., & Velte, C. M. (2024). Optical considerations for designing laser-based volumetric particle tracking velocimetry. *Journal of Fluids Engineering*, 1-13.

Abitan, H., Zhang, Y., Ribergård, S. L., Nielsen, J. S., & Velte, C. M. (2021). Development of optical techniques for large volume ptv measurements. In *14th international symposium on particle image velocimetry - piv21, chicago, illinois, usa, august 1-4.*

Broder, D., & Sommerfeld, M. (2007). Planar shadow image velocimetry for the analysis of the hydrodynamics in bubbly flows. *MEASUREMENT SCIENCE AND TECHNOLOGY*, *18*, 2513–2528.

Buttsworth, D. R., & Ahfock, T. L. (2003). A pulsed led system for schlieren flow visualisation. *Tech Report University of Southern Queensland*, 1-10.

Coldren, L. A., Corzine, S. W., & Masanovic, M. I. (2012). Diode lasers and photonic integrated circuits. In *A phenomenological approach to diode lasers* (pp. 45–87). John Wiley & Sons.

Huhn, F., Schanz, D., Manovski, P., Gesemann, S., & Schröder, A. (2018). Time-resolved large-scale volumetric pressure fields of an impinging jet from dense lagrangian particle tracking. *Experiments in Fluids*, *59*(81), 1-16. doi: 1

Nasibov, H., Balaban, E., Kholmatov, A., & Nasibov, A. (2013). High-brightness, high-power led-based strobe illumination for double-frame micro particle image velocimetry. *Flow Measurement and Instrumentation*, *12*, 12-28.

Piprek, J. (2011). Unified model for the gan led efficiency droop. *Proc. of SPIE Gallium Nitride Materials and Devices VI*, *Gallium Nitride Materials and Devices VI*(16), 1–4.

Piprek, J. (2020). Efficiency models for gan-based light-emitting diodes: Status and challenges. *Materials*, *13*(5174), 1–18.

Schubert, E. F. (2006). *Light-emitting diodes*. Cambridge university Press.

Willert, C., Stasicki, B., Klinner1, J., & Moessner1, S. (2010). Pulsed operation of high-power light emitting diodes for imaging flow velocimetry. *MEASUREMENT SCIENCE AND TECHNOLOGY*, *21*(7), 075402.

Zhang, Y. (2024). *Dynamic insights into non-local energy transfer in non-stationary turbulence: Theory, energy transfer mechanisms, methodology and experiments*. Technical University of Denmark.